PCCP

Accepted Manuscript

This article can be cited before page numbers have been issued, to do this please use: E. Tapavicza, G. D. Bellchambers, J. C. Vincent and F. Furche, *Phys. Chem. Chem. Phys.*, 2013, DOI: 10.1039/C3CP51514A.

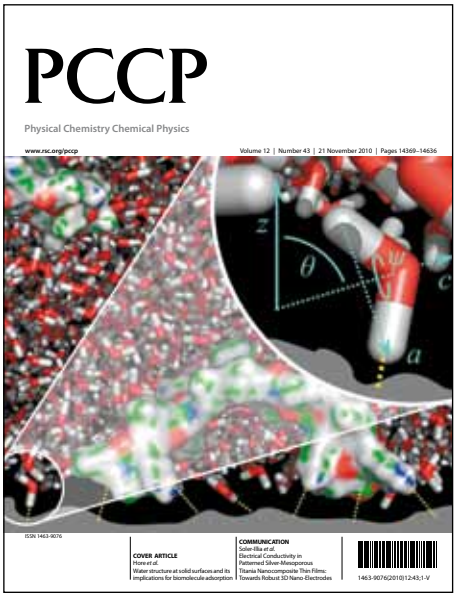

This is an *Accepted Manuscript*, which has been through the RSC Publishing peer review process and has been accepted for publication.

Accepted Manuscripts are published online shortly after acceptance, which is prior to technical editing, formatting and proof reading. This free service from RSC Publishing allows authors to make their results available to the community, in citable form, before publication of the edited article. This *Accepted Manuscript* will be replaced by the edited and formatted *Advance Article* as soon as this is available.

To cite this manuscript please use its permanent Digital Object Identifier (DOI®), which is identical for all formats of publication.

More information about *Accepted Manuscripts* can be found in the **Information for Authors**.

Please note that technical editing may introduce minor changes to the text and/or graphics contained in the manuscript submitted by the author(s) which may alter content, and that the standard **Terms & Conditions** and the **ethical guidelines** that apply to the journal are still applicable. In no event shall the RSC be held responsible for any errors or omissions in these *Accepted Manuscript* manuscripts or any consequences arising from the use of any information contained in them.

View Article Online
DOI: 10.1039/C3CP51514A
ARTICLE TYPE www.rsc.org/xxxxxx | XXXXXXXX

Ab initio non-adiabatic molecular dynamics†

Enrico Tapavicza,[a] Gregory D. Bellchambers,[a] Jordan C. Vincent, [a] and Filipp Furche*[a]

Received Xth XXXXXXXXXX 20XX, Accepted Xth XXXXXXXXX 20XX
First published on the web Xth XXXXXXXXXX 200X
DOI: 10.1039/b000000x

Adiabatic nuclear potential energy surfaces (PESs) defined via the Born–Oppenheimer (BO) approximation are a fundamental concept underlying chemical reactivity theory. For a wide range of excited-state phenomena such as radiationless decay, energy and charge transfer, and photochemical reactions, the BO approximation breaks down due to strong couplings between two or more BO PESs. Non-adiabatic molecular dynamics (NAMD) is the method of choice to model these processes. We review new developments in quantum-classical dynamics, analytical derivative methods, and time-dependent density functional theory (TDDFT) which have lead to a dramatic expansion of the scope of *ab initio* NAMD simulations for molecular systems in recent years. We focus on atom-centered Gaussian basis sets allowing highly efficient simulations for molecules and clusters, especially in conjunction with hybrid density functionals. Using analytical derivative techniques, forces and derivative couplings can be obtained with machine precision in a given basis set, which is crucial for accurate and stable dynamics. We illustrate the performance of surface-hopping TDDFT for photochemical reactions of the lowest singlet excited states of cyclohexadiene, several vitamin D derivatives, and a bicyclic cyclobutene. With few exceptions, the calculated quantum yields and excited state lifetimes agree qualitatively with experiment. For systems with ~ 50 atoms, the present TURBOMOLE implementation allows NAMD simulations with 0.2-0.4 ns total simulation time using hybrid density functionals and polarized double zeta valence basis sets on medium-size compute clusters. We close by discussing open problems and future directions.

1 Introduction

The molecular potential energy surface (PES) is a fundamental concept in chemical science[1]. The notion of a PES is based on the Born-Oppenheimer (BO) approximation[2] which adiabatically separates the electronic and nuclear degrees of freedom. While the BO approximation is generally accurate for molecules in their electronic ground state, it breaks down whenever two or more electronic states are strongly coupled[3]. Many excited state processes such as radiationless decay[4], energy and charge transfer[5], and most photochemical reactions[6] are non-adiabatic, i.e., they involve at least two or more strongly coupled BO PESs. Understanding and controlling non-adiabatic processes is crucial, e.g., for the design of highly efficient sensitizer dyes[7] for photovoltaics or new materials for light-emitting diodes (LEDs)[8] with minimal losses.

The most promising computational approach to fast non-adiabatic processes is non-adiabatic molecular dynamics (NAMD). NAMD simulations directly yield macroscopic observables such as quantum yields or fluorescence intensities. They do not require prior knowledge of the mechanism, which is a key advantage for larger systems with strong couplings where the choice of a reaction coordinate may be difficult or impossible.

[a] *Department of Chemistry, University of California, Irvine, 1102 Natural Sciences II, Irvine, California, 92697-2025, USA. Fax: +1 (949) 824-8571*
* *Tel: +1 (949) 824-5051; E-mail: filipp.furche@uci.edu*

Until recently, realistic NAMD simulations for molecules with more than a few atoms were prohibitively expensive. After all, NAMD simulations require time-integration of the time-dependent Schrödinger equation for nuclei and electrons in some form. This has begun to change due to major advances in three different areas: (i) Efficient approximate NAMD algorithms such as Tully's fewest switches surface hopping (FSSH)[9] that do not require explicit propagation of nuclear wavefunctions. (ii) Forces[10–14] and non-adiabatic couplings[15–23] have become accessible by efficient analytical derivative methods, allowing on-the-fly NAMD simulations[24–30] without the need to compute and store entire PESs. (iii) Excited state energies[13] and non-adiabatic couplings[22] are available at comparatively low cost and reasonable accuracy from time-dependent density functional theory (TDDFT)[31], even for systems with well over 100 atoms. Within plane-wave basis sets, FSSH simulations based on density functional theory (DFT) methods were pioneered by several groups: Doltsinis and Marx[32] used the restricted open-shell Kohn-Sham formalism[33] and Craig et al.[34] implemented a TDDFT based scheme neglecting the exchange-correlation potential[35]. The first linear response TDDFT NAMD implementation was developed by Tapavicza et al.[27] and has been shown to be exact within the Tamm-Dancoff approximation (TDA)[36].

In this perspective, we summarize how developments in the above areas have led to new computational tools greatly ex-

View Article Online
DOI: 10.1039/C3CP51514A

Enrico Tapavicza received his PhD in Theoretical Chemistry from École Polytechnique Fédérale de Lausanne, Switzerland in 2008. Currently he is a postdoc at University of California, Irvine. His research focuses on non-adiabatic molecular dynamics and modelling of photochemical reactions. He will start an appointment as Assistant Professor of Chemistry at California State University, Long Beach, in August 2013.

panding the scope of NAMD simulations. We focus on molecular systems which are most efficiently treated using atom-centered Gaussian basis sets. Perhaps the most important advantage of Gaussian basis set NAMD is that hybrid functionals can be readily used, even for large systems, while they are often prohibitively expensive with plane-wave implementations. Excited state PESs from hybrid TDDFT are considerably more accurate than those from non-hybrid TDDFT[37,38] and may be necessary for even qualitatively correct dynamics in larger systems[28,39,40]. For example, non-hybrid functionals lead to spurious charge transfer intruder states when applied to excited state dynamics of provitamin D[40].

Illustrative applications of NAMD presented here include photochemical reactions of cyclohexadiene, vitamin D derivatives, and previously unpublished results on a cyclobutene derivative, 7,8-dimethylbicyclo[4.2.0]oct-1(6)ene. We close with a discussion of open problems and future directions. This paper reflects our personal perspective on NAMD; for a more complete picture the reader is referred to existing reviews[41–45].

Gregory Bellchambers is a postdoctoral researcher in the group of Professor Furche at the University of California, Irvine. He received his PhD in Theoretical Chemistry from the University of Bristol in 2013. His current research is focused on the development of time-dependent density functional theory methods for non-adiabatic molecular dynamics.

View Article Online
DOI: 10.1039/C3CP51514A

Jordan Vincent is a PhD candidate at the University of California, Irvine (UCI). He received his M.S. in Chemistry from UCI in 2011, and graduated from Saint Cloud State University, in 2007, with a B.S. in Chemistry and B.A. in Mathematics. His research focuses on the development of non-adiabatic molecular dynamics methods in TURBOMOLE, and applications of these methods to study photochemical problems.

Filipp Furche is a Professor of Chemistry at the University of California, Irvine. He received a PhD in Theoretical Chemistry from the University of Karlsruhe, Germany, in 2002. His research focuses on the development of broadly applicable and efficient electronic structure methods such as the random phase approximation, time-dependent density functional methods, and non-adiabatic molecular dynamics. Furche is a core developer of the TURBOMOLE quantum chemistry software.

View Article Online
DOI: 10.1039/C3CP51514A

2 Mixed Quantum-Classical Dynamics

Non-adiabatic molecular dynamics is governed by the time-dependent molecular Schrödinger equation for electrons and nuclei. In mixed quantum-classical dynamics[9], the electronic and nuclear degrees of freedom are separated – electrons evolve according to the time-dependent electronic Schrödinger equation while the nuclei are treated classically. For each nuclear configuration, $\mathbf{R}$, the time-dependent electronic Schrödinger equation determines the time-evolution of the electronic wavefunction $|\Psi(t|\mathbf{R})\rangle$,

$$i\frac{\partial}{\partial t}|\Psi(t|\mathbf{R})\rangle = \hat{H}_{el}(t|\mathbf{R})|\Psi(t|\mathbf{R})\rangle. \quad (1)$$

The time-dependent electronic Hamiltonian,

$$\hat{H}_{el}(t|\mathbf{R}) = \hat{T}_{\mathrm{e}} + \hat{V}_{\mathrm{ee}} + \hat{V}_{\mathrm{en}}(\mathbf{R}) + V_{\mathrm{nn}}(\mathbf{R}) + \hat{V}_{\mathrm{ext}}(t), \quad (2)$$

contains the operator of the kinetic energy of the electrons $\hat{T}_e$, the electron-electron repulsion $\hat{V}_{ee}$, the electron-nucleus attraction $\hat{V}_{en}(\mathbf{R})$, the nucleus-nucleus repulsion $V_{nn}(\mathbf{R})$, and a time-dependent external potential $\hat{V}_{ext}(t)$, e.g., due to a laser field. The nuclear degrees of freedom evolve according to Newton's classical equations of motion,

$$F_j(t) = m_j\ddot{R}_j(t) \quad (3)$$

where $F_j(t)$, m_j, and $\ddot{R}_j(t)$ denote the force, mass, and acceleration, respectively, of the jth nuclear degree of freedom at time t. In mixed quantum-classical dynamics there are two main methods for computing the forces on the nuclei: (i) In Ehrenfest dynamics[46] the forces are computed from the gradient of the time-dependent electronic energy expectation value $\langle E\rangle$. This mean-field method leads to average forces from two or more PESs in regions of weak coupling, which is undesirable for simulating photochemistry[9]. (ii) In the next section we consider the FSSH method wherein the forces are computed as the gradient of single BO PESs, and the non-adiabatic effects arise from the trajectory "hopping" between the PESs in a stochastic manner. Once the forces $F_j(t)$ have been determined, Newton's equations of motion, Eq. (3), may be integrated "on the fly" using standard methods, such as the Leapfrog–Verlet algorithm[47].

3 Surface Hopping in a Basis of Born-Oppenheimer States

In the absence of an external potential, $\hat{V}_{\mathrm{ext}}(t)$, the electronic Hamiltonian reduces to the time-independent BO Hamiltonian with eigenstates $|\Phi_n(\mathbf{R})\rangle$, and their corresponding energies $E_n(\mathbf{R})$ are the PESs. The electronic wavefunction may be expanded in this BO basis,

$$|\Psi(t|\mathbf{R})\rangle = \sum_n c_n(t|\mathbf{R})|\Phi_n(\mathbf{R})\rangle. \quad (4)$$

Insertion of $|\Psi(t|\mathbf{R})\rangle$, Eq. (4), into the time-dependent Schrödinger equation, Eq. (1), yields a coupled matrix equation for the time-dependent amplitude vector $\mathbf{c}$

$$i\dot{\mathbf{c}} = (\mathbf{H} - i\mathbf{Q} + \mathbf{V}_{\mathrm{ext}})\mathbf{c} \quad (5)$$

where $H_{mn} = E_{mn}\delta_{mn}$ are the BO energies, $V_{\mathrm{ext},mn}(t)$ is the coupling due to an external time-dependent potential, and Q_{mn} is the first-order derivative coupling between BO states m and n,

$$Q_{mn} = \langle\Phi_m|\frac{\partial}{\partial t}\Phi_n\rangle = \dot{\mathbf{R}}\cdot\boldsymbol{\tau}_{mn}. \quad (6)$$

The first-order non-adiabatic derivative coupling matrix elements (NACMEs), $\boldsymbol{\tau}_{mn}(\mathbf{R})$, account for the finite kinetic energy of the nuclei:

$$\boldsymbol{\tau}_{mn}(\mathbf{R}) = \langle\Phi_m(\mathbf{R})|\frac{\partial}{\partial\mathbf{R}}|\Phi_n(\mathbf{R})\rangle. \quad (7)$$

At each time step along a trajectory, the instantaneous change in the state populations $|\dot{c}_n|^2$ is computed. For a sufficiently small time step Δt, the transition probability between states m and n is[9]

$$g_{mn} = \frac{2\Delta t}{|c_m|^2}\left[\Im\{c_n^*(H_{nm} + V_{ext,nm})c_m\} - \Re\{c_n^*\dot{\mathbf{R}}\cdot\boldsymbol{\tau}_{nm}c_m\}\right]. \quad (8)$$

A random number, $\zeta \in [0,1]$, is generated and a hop from state m to n ($m \neq n$) occurs if and only if ζ satisfies

$$\sum_{k<n} g_{mk} < \zeta < \sum_{k\leq n} g_{mk}. \quad (9)$$

If a switch is accepted, the velocities of the nuclei are scaled to conserve the total energy – this scaling is chosen to occur along the non-adiabatic coupling vector $\boldsymbol{\tau}_{mn}(\mathbf{R})$.[48–51] Between hops, the individual trajectories evolve on single BO PESs, according to Newton's equations of motion, Eq. (3). Thus, for a trajectory located on BO state m, the nuclei experience forces F_j given by

$$F_j = -\frac{\partial E_m(\mathbf{R})}{\partial R_j}. \quad (10)$$

The FSSH algorithm preserves several desirable features of quantum-classical dynamics[9,52]: If Eq. (5) is integrated continuously, quantum coherence effects in the electronic wavefunction are retained; the fewest switches approach ensures trajectory splitting in regions of strong coupling; within regions of avoided crossings, the method reproduces accurate state populations, given a sufficiently large number of trajectories; total energy conservation is exactly and detailed balance

View Article Online
DOI: 10.1039/C3CP51514A

is approximately satisfied[53]. More rigorous methods which treat the nuclei quantum-mechanically – such as the multiple spawning method[54] – offer higher accuracy than the FSSH method, but the computational cost is significantly greater because explicit propagation of the nuclear wavefunctions is necessary.

4 Time-Dependent Density Functional Theory

In TDDFT[31,55], the exponentially complex many electron problem is mapped onto a system of non-interacting electrons subject to the constraint that the time-dependent electron spin-density, $\rho_\sigma(t,\mathbf{r})$, equals the exact time-dependent spin-density for a given initial state. The non-interacting reference state is a spin unrestricted Slater determinant, Φ^{KS}, of the time-dependent Kohn-Sham (TDKS) spin orbitals $\{|\psi_{j\sigma}(t)\rangle\}$, where $\sigma=\{\alpha,\beta\}$ is a spin index. The total electron density is the sum of up and down spin-densities:

$$\rho(t,\mathbf{r})=\rho_\alpha(t,\mathbf{r})+\rho_\beta(t,\mathbf{r}); \tag{11}$$

$$\rho_\sigma(t,\mathbf{r})= N\sum_{\sigma_2\ldots\sigma_N}\int d^3r_2\ldots\int d^3r_N\left|\Phi^{\mathrm{KS}}(t,\mathbf{r},\sigma,\mathbf{r}_2,\sigma_2,\ldots,\mathbf{r}_N,\sigma_N)\right|^2, \tag{12}$$

where N is the number of electrons. The $\{|\psi_{j\sigma}(t)\rangle\}$ evolve in time according to the TDKS equations,

$$i\frac{\partial}{\partial t}\left|\psi_{j\sigma}(t)\right\rangle=\hat{h}^{\mathrm{KS}}_\sigma\left|\psi_{j\sigma}(t)\right\rangle, \tag{13}$$

where the TDKS one-particle Hamiltonian,

$$\hat{h}^{\mathrm{KS}}_\sigma(t)=\hat{t}+\hat{v}_{\mathrm{en}}+\hat{v}^{\mathrm{H}}[\rho](t)+\hat{v}^{\mathrm{XC}}_\sigma[\rho_\alpha,\rho_\beta](t)+c_x\hat{v}^{\mathrm{X}}_{\mathrm{nl}}[\gamma_\sigma(t)], \tag{14}$$

is the sum of the one-electron operators of the kinetic energy, $\hat{t}$, the electron-nucleus potential $\hat{v}_{\mathrm{en}}$, the Hartree potential,

$$\hat{v}^{\mathrm{H}}[\rho](t,\mathbf{r})=\int d^3r'\frac{\rho(t,\mathbf{r}')}{|\mathbf{r}-\mathbf{r}'|}, \tag{15}$$

the exchange-correlation (XC) potential $\hat{v}^{\mathrm{XC}}_\sigma$ and the nonlocal Fock exchange potential $\hat{v}^{\mathrm{X}}_{\mathrm{nl}}$ with the hybrid mixing coefficient c_x[56]. Within the so-called adiabatic approximation (AA) of TDDFT[57], $\hat{v}^{\mathrm{XC}}_\sigma$ takes the form of the static XC potential evaluated at the time-dependent density:

$$\hat{v}^{\mathrm{XC}}_\sigma[\rho_\alpha,\rho_\beta](t,\mathbf{r})=\left.\frac{\delta E^{\mathrm{XC}}[\rho_\alpha,\rho_\beta]}{\delta\rho_\sigma(\mathbf{r})}\right|_{\rho_{\alpha/\beta}(\mathbf{r})=\rho_{\alpha/\beta}(t,\mathbf{r})}. \tag{16}$$

A number of approximations to the static XC energy functional E^{XC} is available[58,59]. The nonlocal Fock exchange potential is given by

$$\hat{v}^{\mathrm{X}}_{\mathrm{nl}}[\gamma_\sigma]=-\frac{\gamma_\sigma(t,\mathbf{r},\mathbf{r}')}{|\mathbf{r}-\mathbf{r}'|}, \tag{17}$$

where γ_σ is the TDKS density matrix,

$$\gamma_\sigma(t,\mathbf{r},\mathbf{r}')=\sum_j\psi^*_{j\sigma}(t,\mathbf{r})\psi_{j\sigma}(t,\mathbf{r}'). \tag{18}$$

4.1 Linear Response TDDFT

Applying a monochromatic time-dependent perturbation to a molecular system will induce forced oscillations in the electron density. Whenever the frequency, ω, equals an electronic excitation energy, Ω_n, the amplitude of the oscillation diverges, allowing the calculation of excited-state PESs by response theory[60]. Since propagation of Eqs. (5) requires the energies and couplings of several BO states at the same time, linear response TDDFT is the method of choice for NAMD; state-specific iterative methods[61–65] require separate self-consistent treatments for each state.

The transition density matrix, γ_n, between the ground and the n^{th} excited state may be expanded in the basis of unperturbed, real ground-state (GS) KS molecular spin orbitals (MOs) $\phi_{p\sigma}(\mathbf{r})$:

$$\gamma_{n\sigma}(\mathbf{r},\mathbf{r}')=\sum_{ia}\left(X_{nia\sigma}\,\phi_{a\sigma}(\mathbf{r})\phi_{i\sigma}(\mathbf{r}')+Y_{nia\sigma}\,\phi_{i\sigma}(\mathbf{r})\phi_{a\sigma}(\mathbf{r}')\right). \tag{19}$$

Indices $i,j,\ldots$ are used to denote occupied, $a,b,\ldots$ virtual and $p,q,\ldots$ general KS MOs. The transition vectors $\mathbf{X}_n,\mathbf{Y}_n$ are obtained, together with the excitation energies Ω_n, by solution of the TDKS eigenvalue problem[66–69],

$$\left[\begin{pmatrix}\mathbf{A}&\mathbf{B}\\\mathbf{B}&\mathbf{A}\end{pmatrix}-\Omega_n\begin{pmatrix}\mathbf{1}&\mathbf{0}\\\mathbf{0}&-\mathbf{1}\end{pmatrix}\right]\begin{pmatrix}\mathbf{X}_n\\\mathbf{Y}_n\end{pmatrix}=\mathbf{0}, \tag{20}$$

under the symplectic normalization constraint,

$$\mathbf{X}_n^T\mathbf{X}_n-\mathbf{Y}_n^T\mathbf{Y}_n=1. \tag{21}$$

Just as the TDKS density matrix yields the interacting density, the vectors $\mathbf{X}_n,\mathbf{Y}_n$ yield interacting transition densities and Ω_n are interacting excited state energies. The electric and magnetic orbital rotation Hessians are

$$\begin{aligned}(\mathbf{A}+\mathbf{B})_{ia\sigma jb\sigma'}=&(\varepsilon_{a\sigma}-\varepsilon_{i\sigma})\delta_{ij}\delta_{ab}\delta_{\sigma\sigma'}+2(ia\sigma|jb\sigma')\\&+2f^{\mathrm{XC}}_{ia\sigma jb\sigma'}\\&-c_x\delta_{\sigma\sigma'}[(ja\sigma|ib\sigma)+(ab\sigma|ij\sigma)],\\(\mathbf{A}-\mathbf{B})_{ia\sigma jb\sigma'}=&(\varepsilon_{a\sigma}-\varepsilon_{i\sigma})\delta_{ij}\delta_{ab}\delta_{\sigma\sigma'}\\&+c_x\delta_{\sigma\sigma'}[(ja\sigma|ib\sigma)-(ab\sigma|ij\sigma)],\end{aligned} \tag{22}$$

where $\varepsilon_{p\sigma}$ is a GS KS orbital energy eigenvalue, $(ia\sigma|jb\sigma')$ is a two-electron repulsion integral in Mulliken notation, and $f^{\mathrm{XC}}_{ia\sigma jb\sigma'}$ is a matrix element of the exchange-correlation kernel. Within the AA, f^{XC} is given by the second functional

View Article Online
DOI: 10.1039/C3CP51514A

derivative of the static E^{XC} evaluated at the unperturbed, GS density $\rho_\sigma^{\mathrm{GS}}$:

$$f_{\sigma\sigma'}^{\mathrm{XC}}(\mathbf{r},\mathbf{r}') = \left.\frac{\delta^2 E^{\mathrm{XC}}[\rho_\alpha,\rho_\beta]}{\delta\rho_\sigma(\mathbf{r})\delta\rho_{\sigma'}(\mathbf{r}')}\right|_{\rho_{\alpha/\beta}=\rho_{\alpha/\beta}^{\mathrm{GS}}}. \quad (23)$$

Introduction of a basis set allows approximate solution of Eqs. (20) and (21) by linear algebra methods. For finite molecular systems, the GS KS MOs, $\phi_{p\sigma}$, are generally expanded in a basis of atom-centered Gaussian functions, χ_μ:

$$\phi_{p\sigma}(\mathbf{r}) = \sum_\mu C_{\mu p\sigma}\chi_\mu(\mathbf{r}), \quad (24)$$

where $C_{\mu p\sigma}$ are the MO coefficients provided by a GS DFT calculation.

The cost of complete diagonalization of the super matrix in Eq. (20) scales with system size N as $\mathscr{O}(N^6)$ and is prohibitive for systems with more than 10 heavy atoms[70]. However, only the lowest excited states are generally of interest and thus iterative subspace methods may be used[67,68,71–73], for which the rate-determining step is the computation of matrix-vector products

$$\begin{pmatrix}\mathbf{U}\\ \mathbf{V}\end{pmatrix} = \begin{pmatrix}\mathbf{A} & \mathbf{B}\\ \mathbf{B} & \mathbf{A}\end{pmatrix}\begin{pmatrix}\mathbf{X}\\ \mathbf{Y}\end{pmatrix}. \quad (25)$$

This is most efficiently performed as

$$(\mathbf{U}\pm\mathbf{V}) = (\mathbf{A}\pm\mathbf{B})(\mathbf{X}\pm\mathbf{Y}) \quad (26)$$

due to the symmetry of $(\mathbf{A}\pm\mathbf{B})$ and $(\mathbf{X}\pm\mathbf{Y})$ in the atomic orbital (AO) basis[70,74,75]. In integral-direct algorithms, evaluation of the two-electron contribution to Eq. (26) is analogous to a GS KS matrix construction[73]. Highly efficient integral prescreening techniques developed for GS calculations can be applied to excited states with a computational cost that scales asymptotically as $\mathscr{O}(N^2)$. The XC contribution closely resembles an XC potential matrix construction in GS DFT and the efficient quadrature schemes developed for DFT[76,77] can be used to compute this part at $\mathscr{O}(N)$ cost. Resolution of the identity (RI) approximations developed for the GS Coulomb problem[78–84] have also been applied to TDDFT[85,86] and provide an order of magnitude speedup for larger systems with pure density functionals ($c_x = 0$). Use of RI methods for hybrid functionals[87] is more challenging and has so far lead to modest speedups in the range of $2-4$. Pseudospectral methods have also been used to accelerate hybrid calculations by up to an order of magnitude[88].

4.2 Excited-State Energy Gradients in TDDFT

Excited state properties are defined as the derivatives of the excited state energies with respect to an external perturbation, ξ. Of particular relevance here are excited state energy gradients, for which ξ represents a nuclear coordinate. Solution of Eqs. (20) and (21) is equivalent to finding the stationary points of the functional[13,69]

$$G[\mathbf{X},\mathbf{Y},\Omega] = \begin{pmatrix}\mathbf{X}\\ \mathbf{Y}\end{pmatrix}^T\begin{pmatrix}\mathbf{A} & \mathbf{B}\\ \mathbf{B} & \mathbf{A}\end{pmatrix}\begin{pmatrix}\mathbf{X}\\ \mathbf{Y}\end{pmatrix} - \Omega\left[\begin{pmatrix}\mathbf{X}\\ \mathbf{Y}\end{pmatrix}^T\begin{pmatrix}\mathbf{1} & \mathbf{0}\\ \mathbf{0} & -\mathbf{1}\end{pmatrix}\begin{pmatrix}\mathbf{X}\\ \mathbf{Y}\end{pmatrix} - 1\right]. \quad (27)$$

According to the variational principle, derivatives of the transition vectors do not contribute to first-order properties. However, the Ω_n depend implicitly on the MO coefficients through the KS eigenvalues, the two-electron integrals and the XC kernel that appear in the definition of $\mathbf{A}$ and $\mathbf{B}$, Eq. (22). Straightforward differentiation of Eq. (27) thus leads to derivatives of the MO coefficients, $\mathbf{C}^\xi$, with respect to all nuclear degrees of freedom, each requiring the solution of a coupled-perturbed KS (CPKS) equation. With considerable effort, the associated equations may be rearranged and the $\mathbf{C}^\xi$ eliminated[89,90] by application of the $\mathbf{Z}$ vector method[91,92], for which only one CPKS equation must be solved. Alternatively, the coefficient derivatives can be avoided completely by instead optimizing the Lagrangian[13]

$$L[\mathbf{X},\mathbf{Y},\Omega,\mathbf{C},\mathbf{Z},\mathbf{W}] = G[\mathbf{X},\mathbf{Y},\Omega] + \sum_{ia\sigma} Z_{ia\sigma}F_{ia\sigma} - \sum_{pq\sigma,p\le q} W_{pq\sigma}(S_{pq\sigma}-\delta_{pq\sigma}), \quad (28)$$

where $\mathbf{F}$ is the GS KS matrix and $\mathbf{S}$ is the overlap matrix. The additional Lagrange multipliers, $\mathbf{Z}$ and $\mathbf{W}$, constrain the MOs to satisfy the KS equations and to be orthonormal, respectively, for all values of the external perturbation. The implicit dependence on $\mathbf{C}$ present in $\mathbf{G}$ therefore drops out of $\mathbf{L}$ and no derivatives of $\mathbf{C}$ are required for the gradient.

Once $\mathbf{X}$, $\mathbf{Y}$, Ω, $\mathbf{C}$, $\mathbf{Z}$ and $\mathbf{W}$ have been evaluated, derivatives of the excitation energy follow as

$$\begin{aligned}\Omega^\xi &= L^\xi[\mathbf{X},\mathbf{Y},\Omega,\mathbf{C},\mathbf{Z},\mathbf{W}]\\ &= G^{(\xi)}[\mathbf{X},\mathbf{Y},\Omega] + \sum_{ia\sigma} Z_{ia\sigma}F_{ia\sigma}^{(\xi)} - \sum_{pq\sigma,p\le q} W_{pq\sigma}S_{pq\sigma}^{(\xi)}. \quad (29)\end{aligned}$$

Superscript ξ denotes the total derivative with respect to the perturbation, while (ξ) indicates partial differentiation with $\mathbf{C}$ held constant. By solving a single CPKS equation for $\mathbf{Z}$,

$$(\mathbf{A}+\mathbf{B})\mathbf{Z} = -\mathbf{R}, \quad (30)$$

one- and two-particle relaxed difference density matrices, $\mathbf{P}$ and $\mathbf{\Gamma}$, and the energy-weighted relaxed difference density matrix $\mathbf{W}$ can be built and the gradient computed in the AO basis

View Article Online
DOI: 10.1039/C3CP51514A

as

$$\Omega^{\xi} = \sum_{\mu\nu\sigma} \left\{ h^{\xi}_{\mu\nu} P_{\mu\nu\sigma} - S^{\xi}_{\mu\nu} W_{\mu\nu\sigma} + v^{\mathrm{XC}(\xi)}_{\mu\nu\sigma} P_{\mu\nu\sigma} \right\} + \sum_{\mu\nu\kappa\lambda\sigma\sigma'} (\mu\nu|\kappa\lambda)^{\xi} \Gamma_{\mu\nu\sigma\kappa\lambda\sigma'} + \sum_{\mu\nu\kappa\lambda\sigma\sigma'} f^{\mathrm{XC}(\xi)}_{\mu\nu\sigma\kappa\lambda\sigma'} (X+Y)_{\mu\nu\sigma} (X+Y)_{\kappa\lambda\sigma'}. \quad (31)$$

h is the one-electron core Hamiltonian matrix and $\mathbf{v}^{\mathrm{XC}}$ is the exchange-correlation potential matrix. Greek indices are used to denote quantities in the AO basis. The matrix **R** involves third-order functional derivatives and excitation vectors. Explicit expressions for **R**, **P**, **W** and $\mathbf{\Gamma}$ are given in Ref. 13.

The first term on the right hand side of Eq. (31) includes a Hellmann-Feynman contribution[93],

$$\Omega^{\xi\mathrm{HFA}} = \sum_{\mu\nu\sigma} \langle \mu | \hat{h}^{\xi} | \nu \rangle P_{\mu\nu\sigma}. \quad (32)$$

The remaining terms, the so-called Pulay forces[94], correct for the dependence of the basis functions on the nuclear coordinates. The Pulay forces vanish in the complete basis set limit, but are essential for accurate analytical gradients in finite atom-centered basis sets[94]. For plane-wave[14,95] and some real-space[96] implementations of TDDFT, the Hellmann-Feynman theorem applies and Pulay forces do not arise. Eq. (31) has a similar form to the GS gradient expression and, due to the sparsity of the operator derivatives, may be evaluated for all nuclear coordinates at roughly the cost of a single-point GS calculation, i.e. the effective scaling is $\mathscr{O}(N^2)$.

Analytical TDDFT gradients following the Lagrangian approach described above have been implemented in several quantum chemistry codes, including CADPAC[89,90], TURBOMOLE[85], GAUSSIAN[97], Q-Chem[98], ADF[99], GAMESS[100,101] and ORCA[86]. The formalism has been extended to incorporate resolution of the identity approximations[85,86], range-separated exchange-correlation functionals[100–102], and solvation models[97,102].

4.3 Non-adiabatic Couplings from TDDFT

Since interacting wavefunctions are never computed in TDDFT, calculation of the first-order NACMEs, Eq. (7), is not straightforward. However, as first shown by Pauli[103], the first-order NACMEs can be expressed in a Hellmann-Feynman-like form:

$$\tau^{\xi}_{0n} = \frac{1}{\Omega_n} \left\langle \Phi_0 \middle| \hat{V}^{\xi}_{\mathrm{en}} \middle| \Phi_n \right\rangle = \frac{1}{\Omega_n} \sum_{\sigma} \int d^3 r \, \rho_{0n\sigma}(\mathbf{r}) \hat{v}^{\xi}_{\mathrm{en}}(\mathbf{r}), \quad (33)$$

for exact BO eigenstates $|\Phi_0\rangle$, $|\Phi_n\rangle$. τ^{ξ}_{0n} is the ξ-component of the vector $\boldsymbol{\tau}_{0n}(\mathbf{R})$. Chernyak and Mukamel[15] pointed out that, since the interacting excitation energies Ω_n and transition densities ρ_{0n} may be extracted from TDDFT response theory, Eq. (33) establishes a route to TDDFT first-order NACMEs.

As with the excited-state energy gradients, Eq. (33) does not hold for incomplete AO basis sets and Pulay corrections are needed[104]. Pulay terms are essential in calculating energy gradients that are exact derivatives of the approximate energy. Similarly, all Pulay terms must be accounted for in order to obtain τ^{ξ}_{0n} that are the exact derivative couplings of the approximate BO states. Incorrect couplings introduce uncontrolled errors in the integration of the TDKS equations, leading to unphysical dynamics. Furthermore, the basis set convergence of the couplings computed from Eq. (33) is extremely slow, making it prohibitive for large-scale NAMD simulations[22]. Pulay corrections are not needed for plane-wave basis sets[16,19,105].

An expression that correctly generalizes Eq. (33) to finite atom-centered basis sets may be derived from time-dependent response theory by considering the time-evolution of the purely imaginary matrix element

$$C^{\xi}_{\lambda}(t) = \langle \Psi_{\lambda}(t) | \Psi^{\xi}_{\lambda}(t) \rangle \quad (34)$$

under the influence of a periodic perturbation with dimensionless couping strength λ[22]. Analysis of residues of the first-order frequency-dependent response of the interacting and KS C^{ξ}_{λ} yields

$$\tau^{\xi}_{0n} = -\sum_{ia\sigma} (\mathbf{X}-\mathbf{Y})_{nia\sigma} \langle \phi_{a\sigma} | \phi^{\xi}_{i\sigma} \rangle. \quad (35)$$

The MO coupling elements $\langle \phi_{a\sigma} | \phi^{\xi}_{i\sigma} \rangle$ lead to expressions involving the nuclear derivatives of MO coefficients, $\mathbf{C}^{\xi}$. As in the analytical gradient theory, the $\mathbf{C}^{\xi}$ are eliminated through the use of effective density matrices, which in this case are computed directly from the transition vectors; solution of the **Z**-vector equation is not required. The effective densities are analogs of the one-particle density matrix,

$$\tilde{P}_{nia\sigma} = \frac{1}{\Omega_n} (\mathbf{X}+\mathbf{Y})_{nia\sigma}, \quad (36)$$

the energy-weighted one-particle density matrix,

$$\tilde{W}_{nai\sigma} = \varepsilon_{i\sigma} \tilde{P}_{nia\sigma} + \frac{1}{2} (\mathbf{X}-\mathbf{Y})_{nia\sigma}, \quad (37)$$

$$\tilde{W}_{nij\sigma} = \frac{1}{1+\delta_{ij}} H^{+}_{ij\sigma}[\tilde{\mathbf{P}}_n], \quad (38)$$

and the two-particle density matrix, defined in the AO basis as

$$\Gamma_{n\mu\nu\sigma\kappa\lambda\sigma'} = \tfrac{1}{2} (2 \tilde{P}_{n\mu\nu\sigma} D_{\kappa\lambda\sigma'} - c_x \delta_{\sigma\sigma'} [P_{n\mu\lambda\sigma} D_{\kappa\nu\sigma} + P_{n\nu\lambda\sigma} D_{\kappa\mu\sigma}]). \quad (39)$$

View Article Online
DOI: 10.1039/C3CP51514A

D is the GS KS density matrix and $\mathbf{H}^+[\mathbf{V}]$ is

$$H^+_{ij\sigma}[\mathbf{V}] = \sum_{pq\sigma'} \big(2(ij\sigma|pq\sigma') + 2f^{\mathrm{XC}}_{ij\sigma pq\sigma'} - c_x\delta_{\sigma\sigma'}[(iq\sigma|pj\sigma) + (ip\sigma|jq\sigma)]\big)V_{pq\sigma'}, \quad (40)$$

for a general matrix **V**. The final expression for the NACMEs in the AO basis is

$$\tau^\xi_{0n} = \sum_{\mu\nu\sigma}\Big\{h^\xi_{\mu\nu}\tilde{P}_{n\mu\nu\sigma} - S^\xi_{\mu\nu}\tilde{W}_{n\mu\nu\sigma} + v^{\mathrm{XC}(\xi)}_{\mu\nu\sigma}\tilde{P}_{n\mu\nu\sigma}\Big\} + \sum_{\mu\nu\sigma\kappa\lambda\sigma'}(\mu\nu|\kappa\lambda)^\xi\tilde{\Gamma}_{n\mu\nu\sigma\kappa\lambda\sigma'} - \frac{1}{2}\sum_{\mu\nu\sigma}T^\xi_{\mu\nu}(X-Y)_{n\mu\nu\sigma}, \quad (41)$$

which differs to Eq. (31) only in the effective densities and in the last term, where

$$T^\xi_{\mu\nu} = \langle\chi^\xi_\mu|\chi_\nu\rangle - \langle\chi_\mu|\chi^\xi_\nu\rangle. \quad (42)$$

Eq. (42) introduces translational variance to the couplings, which may be corrected through inclusion of electron-translation factors in the BO states[23].

In the limit of a complete basis set, only the term

$$\tau^{\xi\mathrm{HFA}}_{0n} = \sum_{\mu\nu\sigma}\langle\chi_\mu|\hat{v}^\xi_{\mathrm{ne}}|\chi_\nu\rangle\tilde{P}_{n\mu\nu\sigma} \quad (43)$$

remains, which is the basis-set expansion of the exact coupling, Eq. (33). The additional Pulay terms in Eq. (41) account for the dependence of the atom-centered basis on the nuclear coordinates, and the resulting couplings exhibit rapid and smooth basis set convergence[22].

An earlier implementation of NACMEs for atom-centered basis sets by Hu and coworkers[106] recovers some of the Pulay terms in Eq. (41), but neglects effects due to MO coefficient derivatives[22]. Several groups have proposed to directly compute the derivative coupling **Q** (Eq. (6)) by finite differences using auxiliary ground- and excited-state approximate wavefunctions[27,32,34,107]. This approximate method requires smaller time-steps for accurate couplings and is far less efficient than the analytical method described above. In addition, since the NACMEs are not known, the nuclear velocities must be re-scaled isotropically after a hop, making the dynamics less accurate. For the same reason, decoherence corrections[108–112] are difficult to implement in this scheme.

If the couplings and excited state gradients are computed simultaneously, the derivative integrals need to be computed only once and evaluation of NACMEs for all ξ only requires an additional 10% of CPU time. NACMEs obtained from TDDFT with hybrid exchange-correlation functionals typically agree with full configuration interaction results to within 10-20% if the KS reference is stable[22].

5 TDDFT implementation of the fewest switches surface hopping using localized basis sets

In the following we describe the TDDFT version of FSSH (TDDFT-FSSH) as implemented in TURBOMOLE[113], which is based on the Gaussian basis set implementations of DFT[114] and TDDFT[13]. Using the FROG[47] module, the nuclear degrees of freedom of a large number of independent trajectories are propagated classically using the velocity Verlet algorithm[47,115], where $\ddot{\mathbf{R}}(\mathbf{t})$ is computed from either the ground state nuclear forces, if the trajectory is in the ground state, or from the excited state forces if the trajectory is in an excited state. Both ground and excited state forces are computed analytically using the GRAD and the EGRAD modules, respectively. For details of the implementations of the ground state forces see Ref. 114, and for the excited state gradients see section 4.2. At each time step of the classical propagation, Cartesian NAC vectors (NACVs) $\boldsymbol{\tau}_{0k}$ between the excited state k and the ground state are computed using the implementation of Send and Furche[22] (section 4.3). The present implementation does not include couplings between excited states and thus is restricted to dynamics in the ground and first-excited states.

Together with the adiabatic state energies E_0, E_k, $k = 1,2,3,\cdots N$ we are now able to integrate the equations of motion for the state amplitudes **c**, Eqs. (5), of the Born-Oppenheimer expansion, Eq. (4). The integration is carried out using a unitary propagator[116] $\mathbf{U}(t,\Delta t)$

$$\mathbf{c}(t+\Delta) \approx \mathbf{U}(t,\Delta t)\mathbf{c}(t) \quad (44)$$

$$\mathbf{U}(t,\Delta t)\mathbf{c}(t) = \exp(\frac{\mathbf{B}(t)-\mathbf{B}(\Delta t)}{2}\Delta t) \quad (45)$$

$$B_{kl} = \exp(\gamma_{kl})\dot{\mathbf{R}}\cdot\boldsymbol{\tau}_{lk} \quad (46)$$

$$\gamma_{kl} = \int_0^t (E_k - E_l)dt'. \quad (47)$$

Since the BO propagation of the nuclei has no memory of the time evolution of the wavefunction, the phase of the Kohn-Sham orbitals is subject to sudden inversions. A sudden change in the sign of the orbitals leads to an inversion of the NACV directions, resulting in discontinuous evolution of the expansion coefficients. To avoid this artifact, smooth evolution of the orbitals is enforced by projecting the current orbitals $\phi_i(t)$ on to the orbitals of the previous time step $\phi_i(t-\Delta t)$. If $\langle\phi_i(t)|\phi_i(t-\Delta t)\rangle < 0$, the phase of the current orbital $\phi_i(t)$ is inverted.

After the propagation of **c**, the transition probability is evaluated using Eq. (8). Comparison of the probability with a random number decides whether a switch to another adiabatic state is accepted or rejected.

View Article Online
DOI: 10.1039/C3CP51514A

To contain convergence difficulties that arise close to intersections with the ground state, we use the Tamm-Dancoff approximation (TDA) to TDDFT[117], which has been shown to exhibit smaller instability regions on the potential energy surfaces. If a trajectory reaches a singlet instability, which corresponds to a negative excitation energy in TDDFT/TDA, a switch to the ground state is enforced. In order to conserve the total energy after a surface hop, the nuclear velocities are rescaled along the NACV[9]. Previous approaches based on finite differences[27,107] are limited to isotropic velocity rescaling. An ensemble of classical trajectories thus generated should reflect the different reaction branches and products that arise from the splitting of a nuclear wave packet. In addition, a macroscopic ensemble can be simulated by choosing different initial conditions.

Important advantages of the present approach over plane-wave implementations include: i) the use of atom centered basis functions instead of plane waves, ii) all electron calculations instead of pseudopotentials, iii) analytical computation of the NACMEs instead of a finite difference scheme, and iv) a unitary propagation of Eqs. (5) instead of the non-unitary Runge-Kutta integration, which does not conserve the norm of **c**.

6 Applications

The linear response TDDFT-FSSH method has been applied to study a variety photochemical reactions[20,21,27,40,118–120]. The method has been extended to include a classical chemical environment (QM/MM)[121,122] and to include time-dependent external fields[123–125].

In the following we illustrate how TDDFT-FSSH may be used to obtain information about the dynamics of photochemical reactions and how experimental observables can be computed. In particular, we review the dynamics of photoexcited cyclohexadiene, provitamin D (Pro), and previtamin D (Pre)[40], and present a study of the 2+2 ring-opening of a cyclobutene derivative. All non-adiabatic simulations reported here were carried out using the localized basis set implementation described in section 5.

6.1 Computational Details

Unless otherwise stated, the PBE0 exchange correlation functional[126], a hybrid functional with mixing parameter $c_x = 0.25$, was used in all DFT and TDDFT (TDPBE0) calculations. The SVP[127] basis set was employed throughout. For all molecules studied, this basis leads to a systematic blue shift of ≈ 0.2 eV in the excitation energies of the lowest two excited states relative to aug-cc-pVTZ[128,129] calculations. A total of two excited states were computed at each time step, but only coupling between the ground and first excited states was considered in the surface hopping algorithm.

The initial structures of the FSSH trajectories were taken from Boltzmann ensembles at 300 K generated using ground state BO molecular dynamics (BOMD). The Nosé-Hoover thermostat with a characteristic frequency of 500 a.u. was applied. Ground state MD simulations employed a time step of 50 a.u. (≈ 1 fs) for the propagation of the nuclear positions. For Pre, starting structures were generated using replica exchange MD[130]. For each molecule, 50-200 starting geometries and velocities were chosen as starting structures for the TDDFT-FSSH simulations. The molecules were prepared in the first excited state and the nuclear positions were propagated conserving the total energy of the system (NVE). Excited state simulations employed a time step of 40-50 au. FSSH trajectories were propagated for 2-5 ps. For more details on the calculations of CHD and vitamin D derivatives see Ref. 40.

For comparison, excitation energies were calculated via linear-response second-order approximate coupled cluster singles and doubles methods (CC2)[131]. CC2 calculations employed the aug-cc-pVTZ[128,129] basis set and the frozen core approximation.

6.2 Photochemistry of cyclohexadiene

The photoinduced ring-opening of cyclohexadiene (CHD) serves as a prototype reaction to gain basic understanding of the dynamics of the (bio)-synthesis of vitamin D[132] and the mechanism of molecular photo switches[133,134]. Experimentally, the excited state has been found to decay with three different time constants[135,136], $\tau_1 = 21$ fs, $\tau_2 = 35$ fs, $\tau_3 = 80$ fs. The first two experimental constants have been proposed to arise from transitions from the spectroscopic state (B symmetry in the C2 point group) to a dark state (A symmetry), and the third constant has been proposed to arise from the transition from the dark state to the ground state[135,136]. This model is supported by static electronic structure calculations and minimum energy pathway calculations[137,138]. However, knowledge of the potential energy surface does not directly provide information about reaction rates. TDDFT-FSSH simulations of CHD[40] exhibit a biexponential decay, with a fast and slow component ($\tau_1 = 40$ fs, $\tau_2 = 80$ fs). The TDDFT-FSSH simulations suggest that two parallel reaction channels are responsible for the different decay constants rather than sequential events. We find that the fast decay component arises from the fraction of molecules that react to form hexatriene through the ring-opening (*reactive channel*) whereas the slow component arises from a fraction of the molecules that decay without bond breaking (*unreactive channel*). This information is directly available from our simulations but can only be obtained indirectly from experiments.

View Article Online
DOI: 10.1039/C3CP51514A

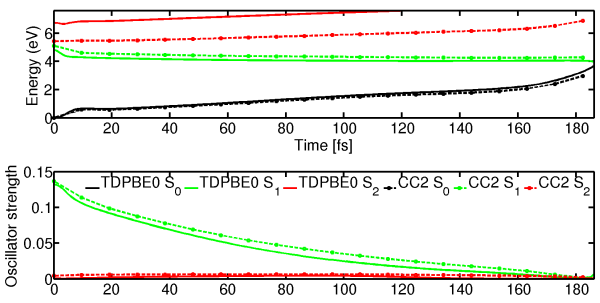

Fig. 1 Low temperature (10 K) MD simulation of cyclohexadiene in the first excited state using nuclear forces obtained from TDPBE0. Upper panel: potential energy curves along the ring-opening coordinate. Lower panel: Time evolution of the the oscillator strengths for $S_0 - S_1$ and $S_0 - S_2$ transition. Solid lines: TDPBE0, dashed lines: CC2; Black: S_0, green: S_1, red: S_2.

NAMD simulations generally break all spatial symmetry and are carried out without symmetry constraints. Thus the transition from the spectroscopic B state to the dark A state predicted by CASSCF minimum energy calculations in C_2 symmetry shows up as a continuous change of the $S_1 - S_0$ oscillator strengths along the reaction path (Fig. 1).

6.3 Photochemistry of provitamin D

The computational efficiency of TDDFT-FSSH has extended the scope of simulations beyond small model systems, such as CHD, to direct simulations of the photochemical ring-opening of Pro, the first step in vitamin D photosynthesis[40] (Fig. 2). Similar to CHD, TDDFT-FSSH simulations of Pro exhibit fast and slow components of excited-state decay, due to reactive and unreactive fractions of the molecules. In the case of Pro, the interpretation of having two parallel decay channels has also been proposed on the basis of experimental findings[141]. The origin of the parallel channels can not yet be determined from experiments. The theory of reactive and unreactive reaction channels with fast and slow excited state decay rates, respectively, still needs to be confirmed experimentally.

The decay of the excited state population can only be measured indirectly by experiment, for instance by probing absorption or emission of the excited state. In the FSSH simulations, the excited state populations are directly available and allow the computation of experimental observables for comparison. For example, the time evolution of the S_1-S_0 oscillator strengths averaged over all trajectories enables calculation of the time-dependent fluorescence of excited Pro (Fig. 3). Similarly, the fluorescence-excitation spectrum (Fig. 4) can be obtained by plotting the time average of the oscillator strengths as a function of the emission frequency. Compared

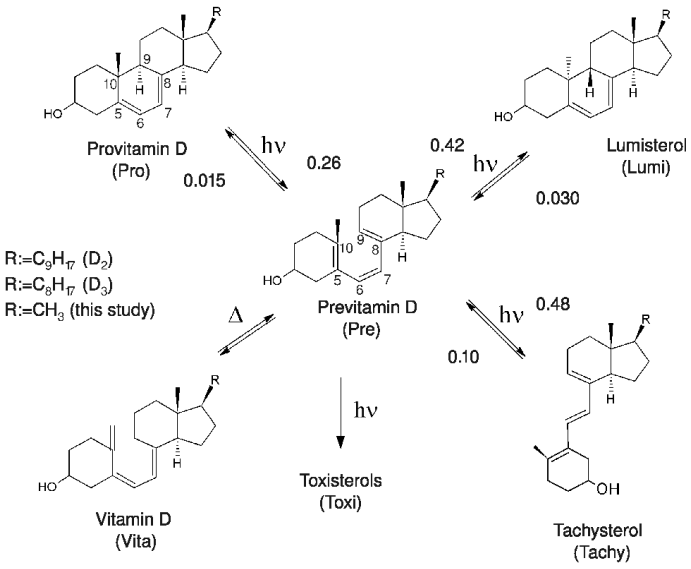

Fig. 2 (Photo)chemical reactions involved in the formation of vitamin D according to Ref.[139]. Quantum yields, measured in ether at 5° C at an excitation wavelength of 253.7 nm[140], are given on the arrows for some reactions.

to the absorption spectrum of Pro (blue in Fig. 4), the emission spectrum (red in Fig. 4) is red shifted. Furthermore, a large decrease in intensity is observed, in agreement with experimental results[141].

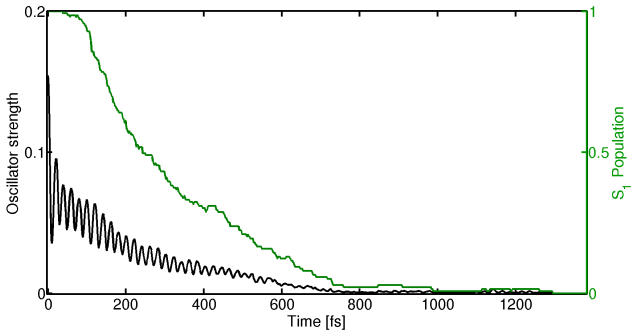

Fig. 3 Time evolution of the oscillator strengths averaged over 139 trajectories of the photoexcited Pro (black). The signal is proportional to the time-dependent fluorescence. In green, the evolution of the S_1 population is shown.

6.4 Photochemistry of previtamin D

Another illustration of the usefulness of TDDFT-FSSH simulations for testing an experimental hypothesis is the wavelength dependent photochemistry of previtamin D (Pre) (Fig. 2): Excitation on the red end of the UV spectrum predomi-

View Article Online
DOI: 10.1039/C3CP51514A

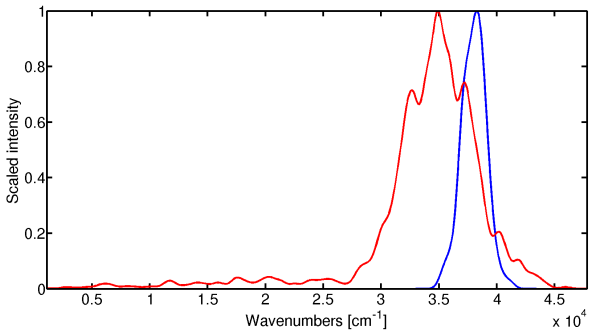

Fig. 4 Absorption (blue) and emission (red) spectra calculated from 139 TDDFT-FSSH trajectories of Pro. For every individual spectrum a Gaussian broadening with a standard deviation of 0.05 eV was applied. The absorption spectrum was obtained by averaging all the spectra of the first time step of the TDDFT-FSSH simulations. The emission spectrum was averaged over the excited state simulation time and over all 139 trajectories.

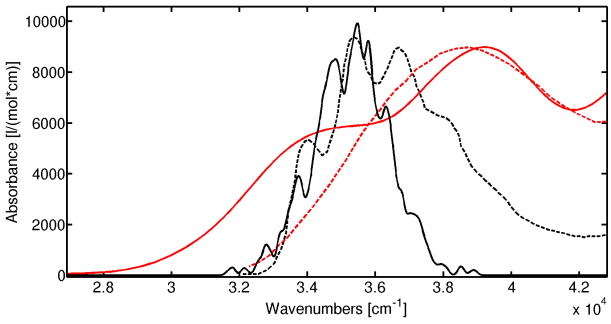

Fig. 5 Experimental (dashed) and theoretical (solid) absorption spectra of Pro (red) and Pre (black). In the case of Pro, excitation energies were averaged over an ensemble of structures obtained from ground state BOMD. For Pre, excitation energies were averaged of an ensemble of structures obtained from REMD. Gaussian broadening with a standard deviation of 0.05eV was applied to each individual spectra. Experimental spectra of Pro and Pre was recorded, in ethanol [143] and methanol, respectively [141]. Calculated intensities were scaled by a factor of 2.58 to match intensity of the maximal absorption band of the experimental spectrum of Pre.

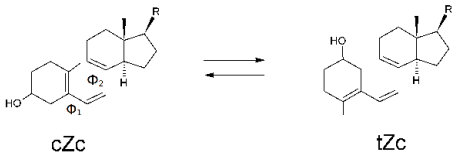

Fig. 6 Rotational isomerization between the two major conformers of previtamin D, cZc and tZc. ϕ_1 and ϕ_2 refer to the dihedral angles defined by C(10)-C(5)-C(6)-C(7) and C(6)-C(7)-C(8)-C(9), respectively. For numbering of the atoms see Fig. 2.

nantly leads to ring-closure, forming Pro or its stereoisomer Lumisterol (Lumi). Excitation on the blue side, in contrast, predominantly leads to the cis-trans isomerization of the central double bond, forming Tachysterol (Tachy). A number of different photoreaction products classified as Toxisterols (Toxi) have also been identified after exposure to UV light on the blue side of the spectrum.

A conformational control mechanism [142] has been suggested as the reason behind this wavelength dependency. To test this hypothesis and to understand the details of the photochemical equilibrium on an atomic level TDDFT-FSSH simulations were performed using different conformers of Pre as initial structures. To sample the Pre conformers with a room-temperature statistical distribution we carried out *ab initio* replica exchange molecular dynamics. The absorption spectrum of Pre was computed as average over single spectra of this ensemble. As in the experiments [141,143], the calculated spectrum of Pre appears with less structure and blue shifted compared to the spectrum of Pro (Fig. 5). More information on the different absorption bands can be obtained by plotting the excitation wavelength as a function of the dihedral angles of each conformer (Figs. 6 and 7). This reveals a characteristic dependence of the excitation wavelengths on the dihedral angle conformation of the molecule.

In a second step, the influence of the dihedral angle conformation of the initial structure on the formation of certain reaction products was investigated. For this purpose we computed TDDFT-FSSH trajectories for 200 initial structures randomly chosen from the ground-state ensemble. The simulations show that photoexcitation of the cZc conformers from the central regions in Fig. 7 ($\phi_1 = [0,90°], \phi_2 = [0,90°]$ and $\phi_1 = [0,-90°], \phi_2 = [-90°,0]$) predominantly lead to ring-closure products Lumi and Pro. This may be rationalized by the vicinity of carbons C(9) and C(10) in the cZc conformation (structures **a** in Figs. 8 and 9), facilitating ring-closure. On average these conformers exhibit lower excitation energies, explaining why low excitation energies lead to ring-closure. Moreover, we see that the stereochemistry of the initial structure determines whether Lumi or Pro is formed: Only molecules in the upper central region ($\phi_1 = [0,90°], \phi_2 = [0,90°]$; example trajectory in Fig. 8) form Lumi (**c** in Fig. 8), while the molecules in the lower central part ($\phi_1 = [0,-90°], \phi_2 = [-90°,0]$; trajectory in Fig. 9) form Pro (**c** in Fig. 9). Molecules with high excitation energies in the upper right region of Fig. 7 lead to double bond isomerization, forming Tachy. Surface hops may occur at different regions on the PES: In the trajectory shown in Fig. 8, the hop is mediated by vibronic coupling, far away from a conical intersection or an avoided crossing. In contrast, in Fig. 9, the surface hop occurs at a conical intersection, i.e. a singlet instability region with negative TDA excitation ener-

View Article Online
DOI: 10.1039/C3CP51514A

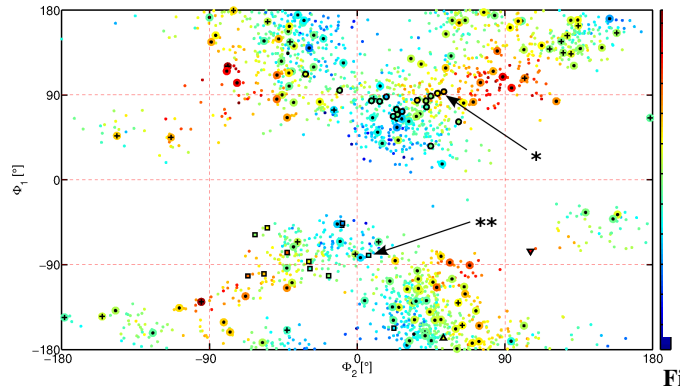

Fig. 7 Relationship between torsional angles ϕ_1 and ϕ_2 of Pre (defined in Fig. 6) and excitation energy and photo product. The color code indicates the excitation energy in eV. Relaxation without photoreaction is indicated by a black dot. Trajectories leading to ring-closure are indicated by squares (Pro formation) or by circles (Lumi formation). Crosses denote Z/E isomerization, yielding tachysterol. Δ denotes hydrogen transfer reaction to vitamin D and ∇ denotes toxisterol formation. * and ** indicate illustrative trajectories shown in Figs. 8 and 9, respectively.

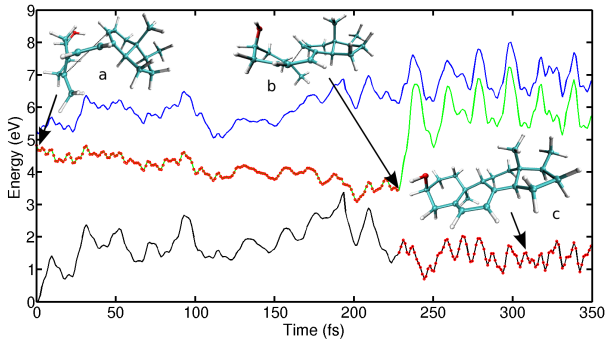

Fig. 8 Illustrative trajectory for the reaction Pre → Lumi. Potential energies are shown as a function of time (black: S_0, green: S_1, and blue: S_2). Red dots indicate the electronic state which is currently populated. Molecular structures **a**, **b**, and **c** are shown for time 0, at the surface hop, and after relaxation to S_0, respectively. At $t = 0$ (structure **a**) Pre exhibits dihedral angles $\phi_1 = 53^\circ$ and $\phi_2 = 94^\circ$ (denoted with $*$ in Fig. 7).

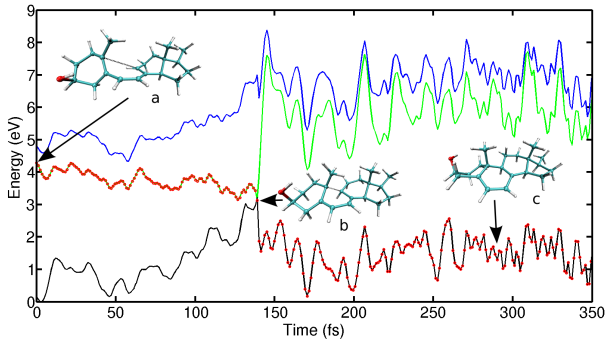

Fig. 9 Illustrative trajectory for the reaction Pre → Pro. See Fig. 8 for details. At $t = 0$ (structure a) Pre exhibits dihedral angles $\phi_1 = 7^\circ$ and $\phi_2 = -80^\circ$ (denoted with $**$ in Fig. 7).

gies. The simulations are consistent with experimental findings. Based on the atomistic picture obtained from the simulations, we are able to confirm the proposed conformational control of the wavelength dependence.

Regarding Tachy formation, the simulations provide further evidence for the Hula-twist mechanism, which has been proposed to explain spectroscopic experiments in a solid matrix [144].

6.5 Cyclobutene photochemistry

Another prototype photoinduced electrocyclic reaction is the the 2+2 ring-opening of cyclobutene. According to the Woodward-Hoffman (WH) rules the photochemical ring-opening follows a disrotatory pathway. For example, for the rigid cyclobutene derivative, 7,8-dimethylbicyclo[4.2.0]oct-1(6)ene (**1**), the allowed products of the cis isomer are E,E-**2** and Z,Z-**2**, whereas the only allowed product of trans-**1** is E,Z-**2** (Fig. 10). However, for most cyclobutene derivatives a large amount of the photochemically forbidden stereoisomer [145–147] is observed. Different explanations of this finding have been proposed, including isomerization in the hot ground state, but subsequently ruled out by experiment [148]. Electronic structure calculations suggest the existence of a number of highly twisted geometries close to the C_2 symmetric S_1 minimum structure, allowing the formation of the photochemically forbidden product [149,150]. Furthermore, it has been argued that through an adiabatic ring-opening an excited WH-allowed product could be formed, which then partially isomerizes to the forbidden product [151]. Fuss et al. [152] suggest that a dynamic effect, i.e., an anti-WH momentum that arises from an initial conrotatory twist of the C-C double bond in the Franck-Condon region, is responsible for the formation of the non-WH product. Since the TDDFT-FSSH approach intrinsically takes into account these effects, we applied the method to investigate these phenomena. To assess the stereochemistry, we simulated 120 FSSH trajectories of each, cis-**1** and trans-**1**. Starting structures were taken from a Boltzmann ensemble at 300K and each FSSH trajectory was simulated for 2 ns. Cis-**1** and trans-**1** decay with time constants of 223 and 159 fs, respectively. In both cases, cis-**1** and trans-**1**, our gas-phase simulations predict the major reaction product that has been found experimentally in solution [146] (Fig. 10). However, in the case of trans-**1**, our calculations suggest the formation of the Z,Z-2

View Article Online
DOI: 10.1039/C3CP51514A

conformer as the anti-WH product, while only the E,E-2 conformer is detected experimentally. Furthermore, a number of side products are found in our simulations (Fig. 11), which have not been reported in the experimental study[146]. This discrepancy could in part be due to the absence of a solvent in our simulations and warrants further study.

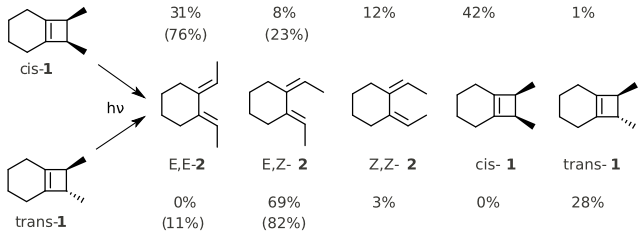

Fig. 10 Calculated quantum yields of the major photoreaction products of cis-**1** and trans-**1**. Experimental quantum yields[146] in solution are shown in parentheses if available.

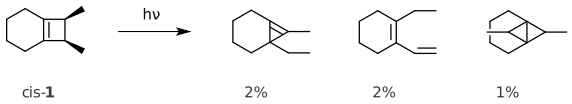

Fig. 11 Calculated quantum yields of the minor photoreaction products of cis-**1.**

7 Conclusion and outlook

NAMD simulations based on TDDFT-FSSH provide detailed mechanistic insight into photochemical processes. For the systems studied here, experimental quantum yields, branching ratios, and excited state lifetimes are qualitatively reproduced with few exceptions. This is very encouraging in view of the size and complexity of these systems. We find that hybrid exchange is crucial for a correct ordering of excited states and thus realistic NAMD. This is consistent with benchmark studies[37,38] showing that hybrid functionals clearly outperform nonhybrid functionals for excitation energies. With the present TURBOMOLE implementation, total simulation times of 0.2 to 0.5 ns are feasible for systems with approximately 50 atoms using hybrid TDDFT and polarized double-zeta basis sets. The possibility to efficiently include exact exchange constitutes the crucial advantage of local-basis-set of TDDFT-FSSH compared to plane-wave implementations. We expect that NAMD simulations using TDDFT-FSSH will prove extremely valuable for the interpretation of pump-probe experiments and will become a routine tool for mechanistic studies in photochemistry. That said, there is ample room for future improvements. First, further benchmarks using both theoretical and experimental reference data are highly desirable to quantify the effect of the various approximations made in TDDFT-FSSH. Second, deficiencies of present day adiabatic TDDFT methods should be quantified and addressed, such as self-interaction error[153], the failure to accurately describe long-range charge-transfer excitations[154], the breakdown for conical intersections[155] with the ground state, and the effects of higher excitations[156]. Third, limitations of FSSH need to be explored further, e.g., by including decoherence. Fourth, the computational efficiency of TDDFT-FSSH can and should be improved by specialized algorithms and by taking advantage of modern parallel architectures. Work along these lines is in progress.

Acknowledgement

This material is based on work supported by the Department of Energy under Award Number DE-SC0008694.

References

1 B. T. Sutcliffe, *Mol. Phys.*, 2006, **104**, 715.
2 M. Born and J. R. Oppenheimer, *Ann. Physik*, 1927, **84**, 457.
3 L. S. Cederbaum, *Conical Intersections: Electronic Structure, Dynamics & Spectroscopy*, World Scientific, Singapore, 2004, vol. 15, ch. 1, p. 3.
4 P. Avouris, W. M. Gelbart and M. A. El-Sayed, *Chem. Rev.*, 1977, **77**, 793.
5 V. May and O. Kühn, *Charge and Energy Transfer Dynamics in Molecular Systems*, Wiley-VCH, Weinheim, 2005.
6 N. J. Turro, *Modern Molecular Photochemistry*, University Science Books, Sausalito, CA 94965, 1991.
7 B. O'Regan and M. Gratzel, *Nature*, 1991, **353**, 737.
8 Q. Peng, Y. Yi, Z. Shuai and J. Shao, *J. Am. Chem. Soc.*, 2007, **129**, 9333.
9 J. C. Tully, *J. Chem. Phys.*, 1990, **93**, 1061.
10 H. Lischka, M. Dallos and R. Shepard, *Mol. Phys.*, 2002, **100**, 1647.
11 E. Ventura, M. Dallos and H. Lischka, *J. Chem. Phys.*, 2003, **118**, 10963.
12 A. Köhn and C. Hättig, *J. Chem. Phys.*, 2003, **119**, 5021.
13 F. Furche and R. Ahlrichs, *J. Chem. Phys.*, 2002, **117**, 7433.
14 J. Hutter, *J. Chem. Phys.*, 2003, **118**, 3928.
15 V. Chernyak and S. Mukamel, *J. Chem. Phys.*, 2000, **112**, 3572.
16 R. Baer, *Chem. Phys. Lett.*, 2002, **364**, 75.
17 H. Lischka, M. Dallos, P. G. Szalay, D. R. Yarkony and R. Shepard, *J. Chem. Phys.*, 2004, **120**, 7322.
18 M. Dallos, H. Lischka, R. Shepard, D. R. Yarkony and P. G. Szalay, *J. Chem. Phys.*, 2004, **120**, 7330.
19 C. Hu, H. Hirai and O. Sugino, *J. Chem. Phys.*, 2007, **127**, 064103.
20 I. Tavernelli, E. Tapavicza and U. Rothlisberger, *J. Chem. Phys.*, 2009, **130**, 124107.
21 I. Tavernelli, E. Tapavicza and U. Rothlisberger, *J. Mol. Struct. THEOCHEM*, 2009, **914**, 22.
22 R. Send and F. Furche, *J. Chem. Phys.*, 2010, **132**, 044107.
23 S. Fatehi, E. Alguire, Y. Shao and J. E. Subotnik, *J. Chem. Phys.*, 2011, **135**, 234105.
24 M. Barbatti, M. Ruckenbauer and H. Lischka, *J. Chem. Phys.*, 2005, **122**, 174307.
25 M. Barbatti, A. J. A. Aquino and H. Lischka, *Mol. Phys.*, 2006, **104**, 1053.
26 I. Antol, M. Eckert-Maksic, M. Barbatti and H. Lischka, *J. Chem. Phys.*, 2007, **127**, 234303.

View Article Online
DOI: 10.1039/C3CP51514A

27 E. Tapavicza, I. Tavernelli and U. Rothlisberger, *Phys. Rev. Lett.*, 2007, **98**, 023001.
28 E. Tapavicza, I. Tavernelli and U. Rothlisberger, *J. Phys. Chem. A*, 2009, **113**, 9595.
29 M. Pederzoli, J. Pittner, M. Barbatti and H. Lischka, *J. Phys. Chem. A*, 2011, **115**, 11136.
30 S. A. Fischer, C. T. Chapman and X. Li, *J. Chem. Phys.*, 2011, **135**, 144102.
31 E. Runge and E. K. U. Gross, *Phys. Rev. Lett.*, 1984, **52**, 997.
32 N. L. Doltsinis and D. Marx, *Phys. Rev. Lett.*, 2002, **88**, 166402.
33 I. Frank, J. Hutter, D. Marx and M. Parrinello, *J. Chem. Phys.*, 1998, **108**, 4060.
34 C. F. Craig, W. R. Duncan and O. V. Prezhdo, *Phys. Rev. Lett.*, 2005, **95**, 163001.
35 N. Maitra, *J. Chem. Phys.*, 2006, **125**, 014110.
36 I. Tavernelli, B. F. E. Curchod and U. Rothlisberger, *J. Chem. Phys.*, 2009, **131**, 196101.
37 D. Jacquemin, V. Wathelet, E. A. Perpete and C. Adamo, *J. Chem. Theory Comput.*, 2009, **5**, 2420.
38 R. Send, M. Kühn and F. Furche, *J. Chem. Theory Comput.*, 2011, **7**, 2376.
39 J. Plötner and A. Dreuw, *Chem. Phys.*, 2008, **347**, 472.
40 E. Tapavicza, A. M. Meyer and F. Furche, *Phys. Chem. Chem. Phys.*, 2011, **13**, 20986.
41 Doltsinis and Marx, *J. Theor. Comput. Chem.*, 2002, **1**, 319.
42 K. Drukker, *J. Comp. Phys.*, 1999, **153**, 225.
43 J. C. Tully, *J. Chem. Phys.*, 2012, **137**, 22A301.
44 M. Casida and M. Huix-Rotllant, *Ann. Rev. Phys. Chem.*, 2012, **63**, 287.
45 B. F. E. Curchod, U. Rothlisberger and I. Tavernelli, *ChemPhysChem*, 2013, **14**, 1314.
46 H.-D. Meyer and W. H. Miller, *J. Chem. Phys.*, 1979, **70**, 3214.
47 S. D. Elliott, R. Ahlrichs, O. Hampe and M. M. Kappes, *Phys. Chem. Chem. Phys.*, 2000, **2**, 3415.
48 M. F. Herman, *J. Chem. Phys.*, 1982, **76**, 2949.
49 M. F. Herman, *J. Chem. Phys.*, 1983, **79**, 2771.
50 M. F. Herman, *J. Chem. Phys.*, 1984, **81**, 754.
51 M. F. Herman, *J. Chem. Phys.*, 1987, **87**, 4779.
52 M. D. Hack, A. M. Wensmann, D. G. Truhlar, M. Ben-Nun and T. J. Martinez, *J. Chem. Phys.*, 2001, **115**, 1172.
53 J. R. Schmidt, P. V. Parandekar and J. C. Tully, *J. Chem. Phys.*, 2008, **129**, 044104.
54 T. J. Martinez, M. Ben-Nun and R. D. Levine, *J. Chem. Phys.*, 1996, **100**, 7884.
55 M. Marques, N. Maitra, F. Nogueira, E. Gross and A. Rubio, *Fundamentals of time-dependent density functional theory*, Springer, Heidelberg, 2012, vol. 837.
56 A. D. Becke, *J. Chem. Phys.*, 1993, **98**, 5648.
57 W. K. Gross and W. Kohn, *Adv. Quantum Chem.*, 1990, **21**, 255.
58 D. Rappoport, N. R. M. Crawford, F. Furche and K. Burke, in *Approximate Density Functionals: Which Should I Choose?*, John Wiley & Sons, Ltd, 2009.
59 K. Burke, *J. Chem. Phys.*, 2012, **136**, 150901.
60 O. Christiansen, P. Jørgensen and C. Hättig, *Int. J. Quantum Chem.*, 1998, **68**, 1.
61 T. Baruah and M. R. Pederson, *J. Chem. Theory Comput.*, 2009, **5**, 834.
62 T. Kowalczyk, S. R. Yost and T. Van Voorhis, *J. Chem. Phys.*, 2011, **134**, 054128.
63 T. Ziegler, M. Krykunov and J. Cullen, *J. Chem. Phys.*, 2012, **136**, 124107.
64 M. Filatov and S. Shaik, *Chem. Phys. Lett.*, 1998, **288**, 689.
65 S. Grimm, C. Nonnenberg and I. Frank, *J. Chem. Phys.*, 2003, **119**, 11574.
66 M. E. Casida, in *Time-Dependent Density Functional Response Theory for Molecules*, ed. D. P. Chong, World Scientific, Singapore, 1995, vol. 1, p. 155.
67 R. Bauernschmitt and R. Ahlrichs, *Chem. Phys. Lett.*, 1996, **256**, 454.
68 R. E. Stratmann, G. E. Scuseria and M. J. Frisch, *J. Chem. Phys.*, 1998, **109**, 8218.
69 F. Furche, *J. Chem. Phys.*, 2001, **114**, 5982.
70 F. Furche and D. Rappoport, *Computational Photochemistry*, Elsevier, 2005, vol. 16, p. 93.
71 E. R. Davidson, *J. Comp. Phys.*, 1975, **17**, 87.
72 M. Crouzeix, B. Philippe and M. Sadkane, *SIAM J. Sci. Comput.*, 1994, **15**, 62.
73 H. Weiss, R. Ahlrichs and M. Häser, *J. Chem. Phys.*, 1993, **99**, 1262.
74 B. Roos, *Chem. Phys. Lett.*, 1972, **15**, 153–159.
75 R. Ahlrichs, W. Meyer and C. E. Dykstra, *Advanced Theories and Computational Approaches to the Electronic Structure of Molecules*, Reidel Dordrecht, 1984, vol. 133, p. 19.
76 O. Treutler and R. Ahlrichs, *J. Chem. Phys.*, 1995, **102**, 346.
77 R. E. Stratmann, G. E. Scuseria and M. J. Frisch, *Chem. Phys. Lett.*, 1996, **257**, 213.
78 K. Eichkorn, O. Treutler, H. hm, M. Hser and R. Ahlrichs, *Chem. Phys. Lett.*, 1995, **240**, 283.
79 K. Eichkorn, O. Treutler, H. hm, M. Hser and R. Ahlrichs, *Chem. Phys. Lett.*, 1995, **242**, 652–660.
80 J. L. Whitten, *J. Chem. Phys.*, 1973, **58**, 4496.
81 B. I. Dunlap, J. W. D. Connolly and J. R. Sabin, *J. Chem. Phys.*, 1979, **71**, 3396.
82 J. W. Mintmire and B. I. Dunlap, *Phys. Rev. A*, 1982, **25**, 88.
83 O. Vahtras, J. Almlöf and M. Feyereisen, *Chem. Phys. Lett.*, 1993, **213**, 514.
84 B. Dunlap, *J. Mol. Struct.: THEOCHEM*, 2000, **529**, 37.
85 D. Rappoport and F. Furche, *J. Chem. Phys.*, 2005, **122**, 064105.
86 T. Petrenko, S. Kossmann and F. Neese, *J. Chem. Phys.*, 2011, **134**, 054116.
87 F. Neese and G. Olbrich, *Chem. Phys. Lett.*, 2002, **362**, 170.
88 C. Ko, D. K. Malick, D. A. Braden, R. A. Friesner and T. J. Martinez, *J. Chem. Phys.*, 2008, **128**, 104103.
89 C. Van Caillie and R. D. Amos, *Chem. Phys. Lett.*, 1999, **308**, 249.
90 C. Van Caillie and R. D. Amos, *Chem. Phys. Lett.*, 2000, **317**, 159.
91 R. M. Sternheimer and H. M. Foley, *Phys. Rev.*, 1953, **92**, 1460.
92 N. C. Handy and H. F. Schaefer, *J. Chem. Phys.*, 1984, **81**, 5031.
93 V. Bakken, T. Helgaker, W. Klopper and K. Ruud, *Mol. Phys.*, 1999, **96**, 653.
94 P. Pulay, *Mol. Phys.*, 1969, **17**, 197.
95 N. L. Doltsinis and D. S. Kosov, *J. Chem. Phys.*, 2005, **122**, 144101.
96 A. Sitt, L. Kronik, S. Ismail-Beigi and J. R. Chelikowsky, *Phys. Rev. A*, 2007, **76**, 054501.
97 G. Scalmani, M. J. Frisch, B. Mennucci, J. Tomasi, R. Cammi and V. Barone, *J. Chem. Phys.*, 2006, **124**, 094107.
98 F. Liu, Z. Gan, Y. Shao, C.-P. Hsu, A. Dreuw, M. Head-Gordon, B. T. Miller, B. R. Brooks, J.-G. Yu, T. R. Furlani and J. Kong, *Mol. Phys.*, 2010, **108**, 2791.
99 M. Seth, G. Mazur and T. Ziegler, *Theor. Chem. Acc.*, 2011, **129**, 331.
100 M. Chiba, T. Tsuneda and K. Hirao, *J. Chem. Phys.*, 2006, **124**, 144106.
101 K. A. Nguyen, P. N. Day and R. Pachter, *Int. J. Quantum Chem.*, 2010, **110**, 2247.
102 N. Minezawa, N. De Silva, F. Zahariev and M. S. Gordon, *J. Chem. Phys.*, 2011, **134**, 054111.
103 W. Pauli, *Handbuch der Physik*, Springer, New York, 1933, vol. 24.
104 M. Tommasini, V. Chernyak and S. Mukamel, *Int. J. Quantum Chem.*,

View Article Online
DOI: 10.1039/C3CP51514A

2001, **85**, 225–238.
105 C. Hu, H. Hirai and O. Sugino, *J. Chem. Phys.*, 2008, **128**, 154111.
106 C. Hu, O. Sugino and Y. Tateyama, *J. Chem. Phys.*, 2009, **131**, 114101.
107 U. Werner, R. Mitrić, T. Suzuki and V. Bonačić-Koutecký, *Chem. Phys.*, 2008, **349**, 319.
108 O. V. Prezhdo, *J. Chem. Phys.*, 1999, **111**, 8366.
109 C. Zhu, S. Nangia, A. W. Jasper and D. G. Truhlar, *J. Chem. Phys.*, 2004, **121**, 7658.
110 J. Bedard-Hearn, R. E. Larsen and B. J. Schwartz, *J. Chem. Phys.*, 2005, **123**, 234106.
111 A. W. Jasper, S. Nangia, C. Zhu and D. G. Truhlar, *Acc. Chem. Res.*, 2006, **39**, 101.
112 J. E. Subotnik and N. Shenvi, *J. Chem. Phys.*, 2011, **134**, 024105.
113 TURBOMOLE *V6.4,* TURBOMOLE *GmbH, Karlsruhe, 2011; available from* `http://www.turbomole.com`.
114 M. Häser and R. Ahlrichs, *J. Comput. Chem.*, 1989, **10**, 104.
115 L. Verlet, *Phys. Rev.*, 1967, **159**, 98.
116 M. Barbatti, G. Granucci, M. Persico, M. Ruckenbauer, M. Vazdar, M. Eckert-Maksic and H. Lischka, *J. Photochem. Photobiol. A: Chem.*, 2007, **190**, 228.
117 S. Hirata and M. Head-Gordon, *Chem. Phys. Lett.*, 1999, **314**, 291.
118 E. Tapavicza, I. Tavernelli, U. Rothlisberger, C. Filippi and M. E. Casida, *J. Chem. Phys.*, 2008, **129**, 124108.
119 R. Mitric, U. Werner and V. Bonačić-Koutecky, *J. Chem. Phys.*, 2008, **129**, 164118.
120 T. Fuji, Y.-I. Suzuki, T. Horio, T. Suzuki, R. Mitric, U. Werner and V. Bonačić-Koutecký, *J. Chem. Phys.*, 2010, **133**, 234303.
121 I. Tavernelli, B. F. Curchod and U. Rothlisberger, *Chem. Phys.*, 2011, **391**, 101.
122 G. Tomasello, M. Wohlgemuth, J. Petersen and R. Mitri, *J. Phys. Chem. B*, 2012, 8762.
123 R. Mitric, J. Petersen, M. Wohlgemuth, U. Werner and V. Bonačić-Koutecky, *Phys. Chem. Chem. Phys.*, 2011, **13**, 8690.
124 R. Mitrić, J. Petersen, M. Wohlgemuth, U. Werner, V. Bonačić-Koutecký, L. Wöste and J. Jortner, *J. Phys. Chem. A*, 2011, **115**, 3755.
125 B. F. E. Curchod, T. J. Penfold, U. Rothlisberger and I. Tavernelli, *Phys. Rev. A*, 2011, **84**, 042507.
126 J. P. Perdew, M. Ernzerhof and K. Burke, *J. Chem. Phys.*, 1996, **105**, 9982.
127 A. Schäfer, H. Horn and R. Ahlrichs, *J. Chem. Phys.*, 1992, **2571**, 97.
128 T. H. J. Dunning, *J. Chem. Phys.*, 1989, **90**, 1007.
129 R. A. Kendall, T. H. J. Dunning and R. J. Harrison, *J. Chem. Phys.*, 1992, **96**, 6796.
130 Y. Sugita and Y. Okamoto, *Chem. Phys. Lett.*, 1999, **314**, 141.
131 O. Christiansen, H. Koch and P. Jørgensen, *Chem. Phys. Lett.*, 1995, **243**, 409.
132 M. F. Holick, *J. Cell. Biochem.*, 2003, **88**, 296.
133 N. L. Rangel, K. S. Williams and J. M. Seminario, *J. Phys. Chem. A*, 2009, **113**, 6740.
134 J. Buback, P. Nuernberger, M. Kullmann, F. Langhojer, R. Schmidt, F. Wurthner and T. Brixner, *J. Phys. Chem. A*, 2011, **115**, 3924.
135 W. Fuss, W. E. Schmid and S. A. Trushin, *J. Chem. Phys.*, 2000, **112**, 8347.
136 K. Kosma, S. A. Trushin, W. Fuss and W. E. Schmid, *Phys. Chem. Chem. Phys.*, 2009, **11**, 172.
137 M. Garavelli, P. Celani, M. Fato, M. J. Bearpark, B. R. Smith, M. Olivucci and M. A. Robb, *J. Phys. Chem. A*, 1997, **101**, 2023.
138 A. Nenov, P. Kölle, M. A. Robb and R. de Vivie-Riedle, *J. Org. Chem.*, 2010, **75**, 123.
139 A. Braun, M. Maurette and E. Oliveros, *Photochemical technology*, Wiley, 1991.
140 E. Havinga, *Cellular and Molecular Life Sciences*, 1973, **29**, 1181.
141 K.-C. Tang, A. Rury, M. B. Orozco, J. Egendorf, K. G. Spears and R. J. Sension, *J. Chem. Phys.*, 2011, **134**, 104503.
142 J. K. Whitesell, M. A. Minton and V. D. Tran, *J. Am. Chem. Soc.*, 1989, **111**, 1473.
143 I. Terenetskaya, *Talanta*, 2000, **53**, 195.
144 A. M. Mueller, S. Lochbrunner, W. E. Schmid and W. Fuss, *Angew. Chem. Intl. Ed.*, 1998, **37**, 505.
145 K. B. Clark and W. J. Leigh, *J. Am. Chem. Soc.*, 1987, **109**, 6086.
146 W. J. Leigh and K. Zheng, *J. Am. Chem. Soc.*, 1991, **113**, 4019.
147 W. J. Leigh and J. A. Postigo, *J. Am. Chem. Soc.*, 1995, **117**, 1688.
148 B. H. O. Cook, W. J. Leigh and R. Walsh, *J. Am. Chem. Soc.*, 2001, **123**, 5188.
149 F. Bernardi, M. Olivucci, I. N. Ragazos and M. A. Robb, *J. Am. Chem. Soc.*, 1992, **114**, 2752.
150 P. Celani, F. Bernardi, M. Olivucci and M. A. Robb, *J. Chem. Phys.*, 1995, **102**, 5733.
151 W. J. Leigh, *Chem. Rev.*, 1993, **93**, 487.
152 W. Fuss, W. E. Schmid, S. A. Trushin, P. S. Billone and W. J. Leigh, *ChemPhysChem*, 2007, **8**, 592.
153 J. P. Perdew and A. Zunger, *Phys. Rev. B*, 1981, **23**, 5048.
154 A. Dreuw, J. Weisman and M. Head-Gordon, *J. Chem. Phys.*, 2003, **119**, 2943.
155 B. G. Levine, C. Ko, J. Quenneville and T. J. Martinez, *Mol. Phys.*, 2006, **104**, 1039.
156 N. T. Maitra, F. Zhang, R. J. Cave and K. Burke, *J. Chem. Phys.*, 2004, **120**, 5932.

View Article Online
DOI: 10.1039/C3CP51514A

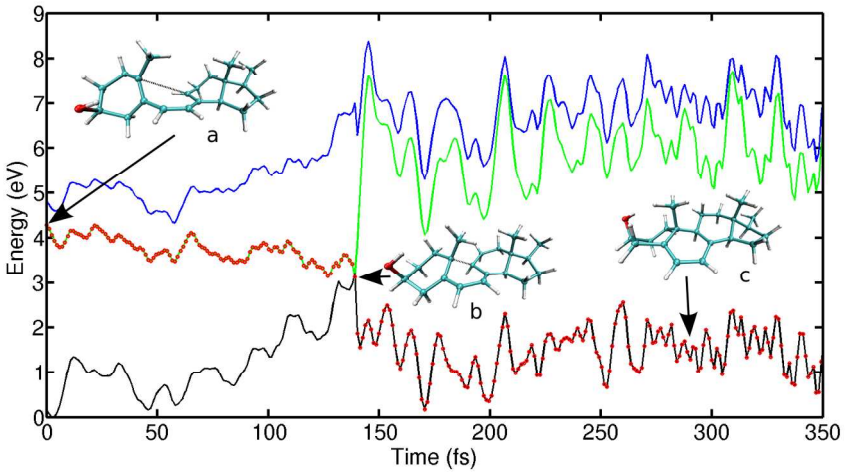

677x337mm (72 x 72 DPI)